09.1

Features of interference phenomena in ZnO films obtained by the magnetron deposition method

© A.M. Ismailov[1], A.E. Muslimov[2]

[1] Dagestan State University, Makhachkala, Dagestan Republic, Russia
[2] National Research Center, „Kurchatov Institute“, Moscow, Russia
E-mail: egdada@mail.ru

Received June 5, 2023
Revised September 7, 2023
Accepted October 2, 2023

The processes of controlled texturing of ZnO films on the *r*-r-plane with a gold buffer layer were studied, taking into account the free potential during magnetron deposition and interference phenomena. It has been shown that, depending on the position of the substrate in the discharge volume, both smooth [001]-textured (single layer) and rough bi-textured (bi-layer) ZnO films can be formed. The classical interference pattern is observed only in smooth textured films. Thus there is the perspective that synthesized transparent film structures based on ZnO can be used as interference sensors for assessing the refractive index of the environment.

Keywords: ZnO, magnetron deposition, interference, refractive index sensor.

DOI: 10.61011/0000000000

Refraction index sensors, which are highly sensitive to changes in the refraction index of the environment, are widely used in a wide variety of industrial applications. The sensor sensitivity is determined by the material used as well as its constructional features, which determines its cost and labor intensity. The use of interference sensors (IS), in which the fringe pattern parameters are directly related to the refraction index of the surrounding medium, seems to us to be underestimated. Despite the low sensitivity, ISs can compete with two-dimensional photonic crystals [1], planar ring resonators [2], micro-spherical ring resonators [3], whose sensitivity does not exceed 250 nm/RIU (RIU — Refraction index unit [4]). For example, in the task of monitoring the degree of pollution of aquatic environments, real-time estimation of pollutant concentration is required. Preliminary calculations show that ISs have sufficient sensitivity when studying photodegradation processes of optically dense solutions, e.g. antibiotics (Refraction index 1.53−1.58). The simplest example of an IS is a ZnO film on double-sided polished Al_2O_3 with a semitransparent gold sublayer. ZnO is characterized by high biocompatibility [5], and ISs based on it can find applications in modern biotechnology.

All synthesis technologies inherently depend on the structure and properties of objects and materials on the conditions of their production. Thus, when creating ISs, it is important to take into account the influence of synthesis conditions on the texture, surface roughness of the films and, as a consequence, on the peculiarities of interference phenomena in them. In balanced magnetron sputtering system with ring concentric magnets, the generated plasma is localized near the target surface. Due to the much higher mobility of electrons, their flow towards the substrate prevails over the ion flow, and the substrate is negatively charged. Therefore, due to the high spatial heterogeneity of the plasma, its electrostatic potential depends on the location of the substrate relative to the magnetron. The influence of electric field on the processes of deposition of metal films is known [6]: increase of diffusion activity of adatoms, coalescence of islands at earlier stages, improvement of the structure of the growing film. Due to the crystal structure of (0001)-grain-oriented ZnO films, they grow even on non-orienting substrates [7]. At the same time, an excess of zinc in the gas phase [8] is required to obtain an epitaxial ZnO film, taking into account the optimal configuration ratio in the film-substrate system. This makes it possible to obtain ZnO films with mono- and biaxial textures in a single experiment by placing substrates of specific orientation in certain positions relative to the magnetron.

In work, the processes of controlled texturing of ZnO films on *r*-plane Al_2O_3 with buffer layers of gold taking into account the free potential, as well as interference phenomena in them, have been studied. The translucent gold sub-layer acted as a highly reflective coating. The cathodoluminscescence in a sapphire sample excited by a stream of fast electrons was used as a source of radiation.

The *r*-plane Al_2O_3 was used as substrates. The front side of the substrates was processed by chemical-mechanical method, the back side — by mechanical method. A gold layer with a thickness of about 200 nm was previously deposited on the substrate by thermal deposition. The substrate was then heated at 730°C to form a porous gold film. ZnO films were deposited by magnetron sputtering at 810° C in an oxygen atmosphere at a pressure of 1.33 Ra on an industrial WATT AMK MI unit. A ZnO ceramic target was used. Constant discharge current 100 mA, deposition time 25 min, film growth rate $\sim$ 2 nm/s. The free potential was measured with an electrostatic voltmeter using probes

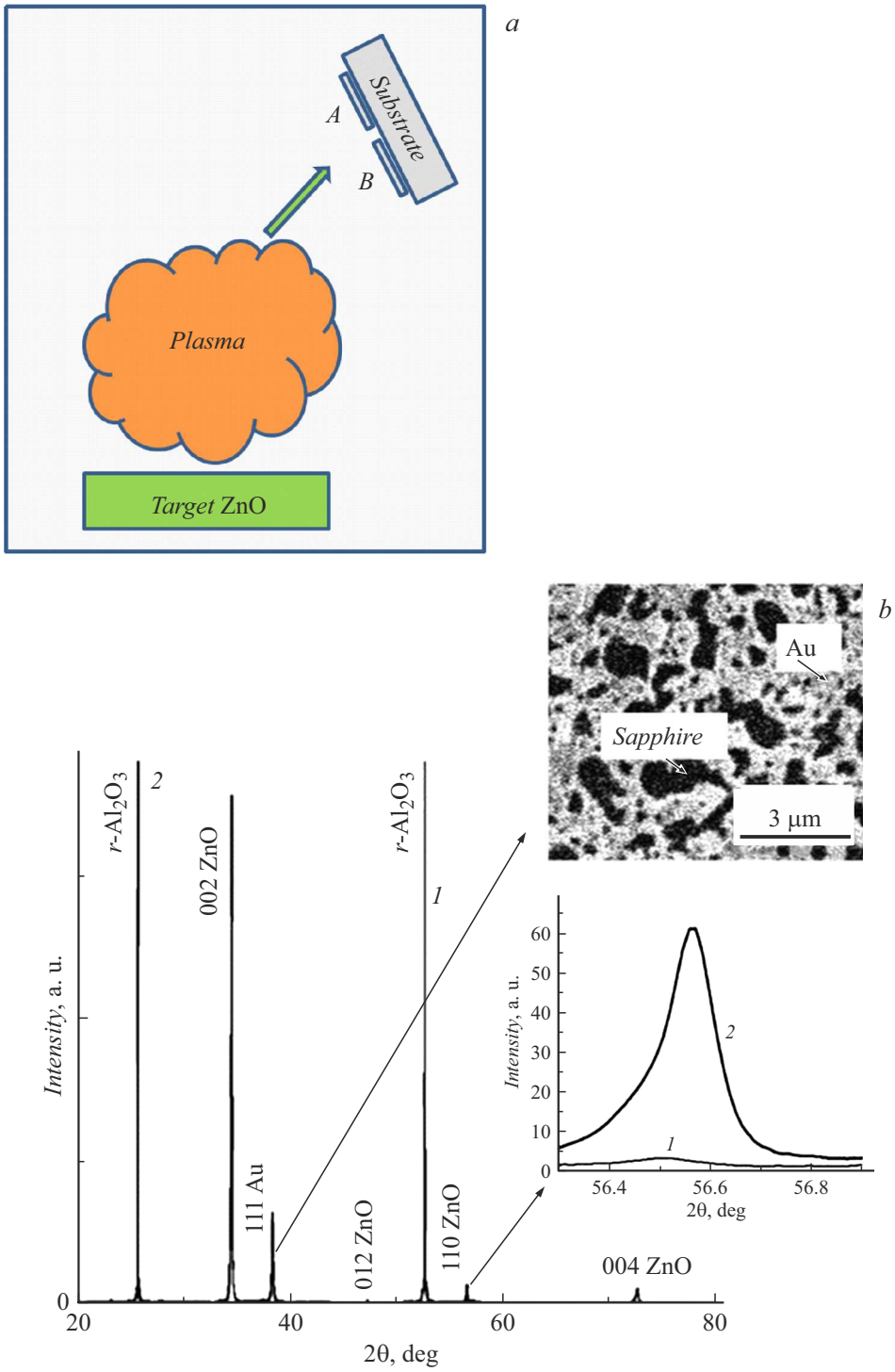

Figure 1. *a* — layout of Al_2O_3 substrates relative to the ZnO target in the magnetron system. The dots I*A* and *B* indicate the locations of the free potential probes. *b* — X-ray diffraction patterns of *A* (curve *1*) and *B* (curve *2*) ZnO films on the *r*- plane Al_2O_3 with a buffer layer of gold. In the upper insert — microscopic image of the surface of the porous gold film, in the lower — the reflex (110) of ZnO on an enlarged scale.

placed at points *A*, *B* (Fig. 1, *a*) at a distance of 5 mm from each other. The grounded anode of the magnetron system served as the reference electrode. The following free potential values were obtained under the above process conditions: at $A \sim 9-12$ V, at $B \sim 16-18$ V.

X-ray diffraction method was used for structural studies of the films. X-ray diffractograms were obtained on an Empyrean diffractometer from PANalytical (Netherlands) in Bragg-Brentano geometry. Radiation from a copper anode ($CuK_{\alpha 2}$- radiation, $\lambda = 1.54$ Å) was used. The High Score

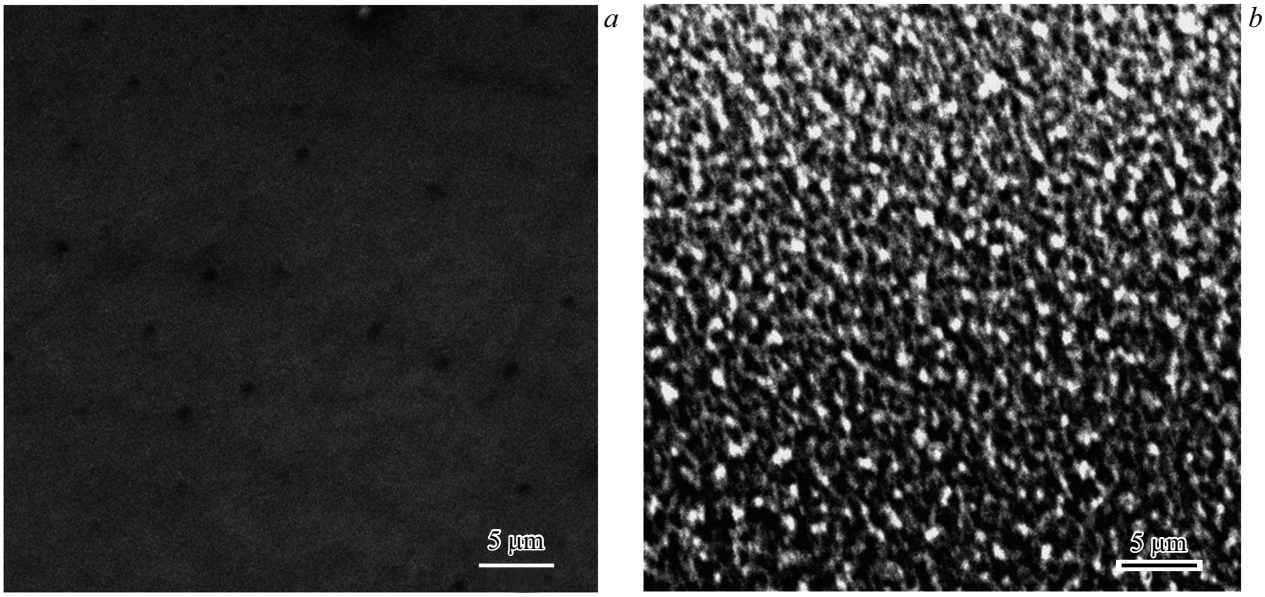

Figure 2. SEM image of the surface of ZnO film of *A* (a) and *B* (*b*) types. Scan size $40 \times 40\,\mu$m.

Plus software and the ICSD (PDF-2) database were used to analyze the diffraction patterns and identify peaks. The interference phenomena in the samples were studied using an Avantas spectrometer (AvaSpec-1024). The radiation source was the cathodoluminscescence in the sapphire sample during exposure to the electron beam. Electron irradiation was performed from the front side of the ZnO film at an 45° angle to the normal. Microscopic studies of a transversely cleaved sample were carried out with a Jeol Neoscope 2 (JCM-6000) scanning-electron microscope (SEM).

ZnO films (hereafter designated as samples of type *A* and *B*, respectively) with thicknesses of the order of $3\,\mu$m, were grown at two locations *A* and *B* in a single deposition process when the r-Al_2O_3 substrates were arranged with a gold buffer layer. According to the X-ray diffraction data (Fig. 1, *b*) on r-plane Al_2O_3 in the process of post-treatment heat treatment, [111]-grain-oriented gold film is formed: in crystals with face-centered cubic structure, the plane (111), which has the highest density of atoms, has the highest growth rate. Due to the weak adhesion of gold to Al_2O_3, a porous gold film is formed (Fig. 1, *b*, upper inset) with a high proportion of uncovered sapphire surface. The growth of ZnO films on r- plane Al_2O_3 with (111) Au buffer layer depends on the conditions near the surface. C position of lattice structural and geometric similarity, which determines epitaxial growth, the minimum parameter mismatch along [001] ZnO and $[\bar{1}11]$ Al_2O_3 ((5.2069−5.1272 Å)/5.1272 Å) is of the order of 1.55%. Thus, at high adatom diffusivity, the epitaxial relationship $(110)[001]\mathrm{ZnO}\|(1\bar{1}\bar{2})[\bar{1}11]\mathrm{Al_2O_3}$ should be fulfilled between the growing ZnO film and r-plane Al_2O_3 . This explains the presence of [110]-crystallites in ZnO films (Fig. 1, *b*, lower insert), which sprout from pores in the Au film and are more significantly represented in the *B* type film. Nevertheless, the bulk of the film according to X-ray diffraction data (Fig. 1, *b*) is grain-oriented along ⟨001⟩. The free potential directly in the probe (substrate) region is determined by the ratio of ion and electron fluxes to the probe. Since the plasma is assumed to be quasi-neutral and the mobility of electrons is much greater than that of ions, the free potential depends mainly on the electron energy [9]. In [10], the correlation between the free potential distribution and electron temperature is confirmed: high electron temperature is characterized by regions with high potential. When the concentration of Zn^{2+} increases and the diffusion activity of adatoms increases, the epitaxial growth of ZnO with the smallest parameter mismatch [8] is realized. Thus, the influence of the substrate electric field on the processes of nucleation and growth of ZnO crystallites can be attributed to the increased flux of Zn^{2+} towards the negatively charged substrate. In this case, the ratio of adatoms Zn^{2+}/O^{2-} increases in the growth zone, and increased diffusion activity of adatoms due to energy transfer to them by „hot“ electrons is observed in the regions with high potential. The above features favor the formation and growth of [110]-crystallites at the initial stage of growth of ZnO films (lower inset in Fig. 1, *b*). Subsequently, in the lower potential region (*A* region), their growth is suppressed at an early stage by [001] -crystallites (curve *1* in Fig. 1, *b*). In the region with a higher potential (*B* region), due to higher diffusion activity, the growth of [110] -crystallites is interrupted at a later stage (curve *2* in Fig. 1, *b*). Suppression of [110]-crystallites at an early stage leads to the formation of a generally homogeneous [001]-grain-oriented ZnO film (Fig. 2, *a*) with lower surface roughness. In the case of ZnO film (*B* region), the processes are complicated by the non-simultaneous transition to (001)-texturing in different

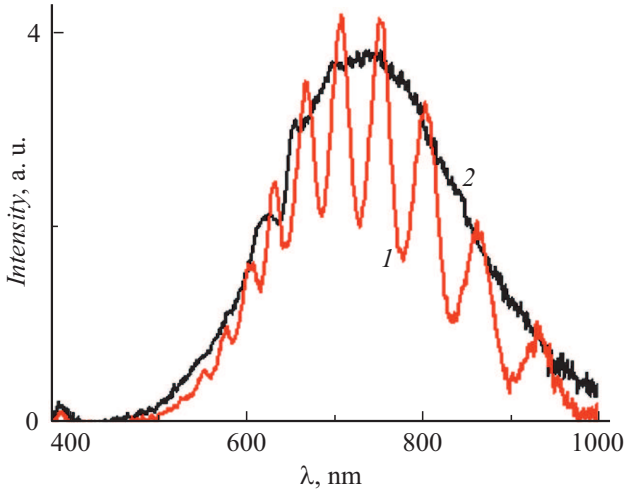

Figure 3. Cathodoluminscescence spectrum of ZnO film on Al_2O_3. *1* — sample type *A*, *2* — sample type *B*.

growth zones (Fig. 2, *b*) of due to the heterogeneity of nucleation conditions. A rough bitextured film with two crystallite orientations is generally formed: (110) and (001). Comparison of the lattice constants of the obtained ZnO structures with those of bulk ZnO [11] also demonstrates the presence of excess zinc in the growth region. Fig. 3 shows the cathodoluminscescence spectra of *A* and *B* samples. The spectra contain weakly intense bands of edge (389 nm) and defect (500−700 nm) luminescence of ZnO, as well as an intense broad band of 600−1000 nm luminescence Al_2O_3, associated with impurity Ti^{3+}. Thus, the luminescence centers are located both in the film thickness and in the substrate Al_2O_3. The curve *1* (type *A*) exhibits oscillations resulting from classical interference, as confirmed by the thickness estimate of 2.9 μm. At the same time, oscillations are absent on the curve *2* (type *B*). To observe a classical fringe pattern in films, it is necessary to minimize the scattering factor at the interfaces. A reflection [12] model can be used to analyze the surface scattering factor:

$$R = R_0 e^{-4\pi R_q/\lambda^2} + \alpha R_d,$$

where R — reflectance of rough surface, R_0 — reflectance of smooth surface, R_d — diffuse scattering coefficient, α — coefficient of proportionality, R_q — RMS roughness, λ — wavelength. At high values of R_q (type *B*), diffuse scattering plays the main role and the interference conditions are broken. For the *B* type sample, diffuse scattering is likely to be observed for both the upper film boundary and the blurred texture boundary in the bitextured film volume.

Thus, the processes of controlled texturing of ZnO films on *r*-plane Al_2O_3 with gold buffer layers considering free potential during magnetron deposition and interference phenomena in them have been investigated in this work. It is shown that both smooth [001]-grain-oriented and rough bitextured ZnO films can be formed depending on the position of the substrate in the discharge volume. The growth features are attributed to the directional flow of Zn^{2+} to the negatively charged substrate, the increased ration of adatoms Zn^{2+}/O^{2-}, and the increased diffusion activity of adatoms in regions of high potential due to energy transfer from high-energy electrons. The classical fringe pattern is observed only in smooth grain-oriented films. The most intense luminescence centers were located in the substrate Al_2O_3, which confirms the possibility of using ICs based on smooth ZnO film under illumination from both front and back sides. The parameters of the fringe pattern depend on the film thickness, and hence further improvements in IS precision are possible.

Funding

The work was performed within the framework of the state assignment National Research Center „Kurchatov Institute,“, Moscow, Russia.

Conflict of interest

The authors declare that they have no conflict of interest.

References

[1] E. Chow, A. Grot, L.W. Mirkarimi, M. Sigalas, G. Girolami, Opt. Lett., **29** (10), 1093 (2004). DOI: 10.1364/ol.29.001093
[2] C.A. Barrios, K.B. Gylfason, B. Sánchez, A. Griol, H. Sohlström, M. Holgado, R. Casquel, Opt. Lett., **32** (21), 3080 (2007). DOI: 10.1364/OL.32.003080
[3] N.M. Hanumegowda, C.J. Stica, B.C. Patel, I. White, X. Fan, Appl. Phys. Lett., **87** (20), 201107 (2005). DOI: 10.1063/1.2132076
[4] Z. Li, L. Hou, L. Ran, J. Kang, J. Yang, Sensors, **19** (18), 3820 (2019). DOI: 10.3390/s19183820
[5] E. Obeng, J. Feng, D. Wang, D. Zheng, B. Xiang, J. Shen, Front. Chem., **10**, 1054739 (2022). DOI: 10.3389/fchem.2022.1054739
[6] K.L. Chopra, J. Appl. Phys., **37** (6), 2249 (1966). DOI: 10.1063/1.1708795
[7] M. Soylu, M. Coskun, J. Alloys Compd., **741**, 957 (2018). DOI: 10.1016/j.jallcom.2018.01.079
[8] T. Trautnitz, R. Sorgenfrei, M. Fiederle, J. Cryst. Growth, **312** (4), 624 (2010). DOI: 10.1016/j.jcrysgro.2009.12.011
[9] A.A. Solov'ev, N.S. Sochugov, K.V. Oskomov, S.V. Rabotkin, Plasma Phys. Rep., **35** (5), 399 (2009). DOI: 10.1134/S1063780X09050055.
[10] D.J. Field, S.K. Dew, R.E. Burrell, J. Vac. Sci. Technol. A, **20** (6), 2032 (2002). DOI: 10.1116/1.1515800
[11] D.D. Yanti, E. Maryanti, J. Sci. Appl. Technol., **5** (1), 198 (2021). DOI: 10.35472/jsat.v5i1.372
[12] H. Davies, Proc. Inst. Electr. Eng., **101**, 209 (1954).

Translated by J.Deineka